Physics Letters B 807 (2020) 135568

Contents lists available at ScienceDirect

Physics Letters B

www.elsevier.com/locate/physletb

Static quadrupole moments of nuclear chiral doublet bands

Q.B. Chen [a,*], N. Kaiser [a], Ulf-G. Meißner [b,c,d], J. Meng [e,f]

[a] Physik-Department, Technische Universität München, D-85747 Garching, Germany
[b] Helmholtz-Institut für Strahlen- und Kernphysik and Bethe Center for Theoretical Physics, Universität Bonn, D-53115 Bonn, Germany
[c] Institute for Advanced Simulation, Institut für Kernphysik and Jülich Center for Hadron Physics, Forschungszentrum Jülich, D-52425 Jülich, Germany
[d] Ivane Javakhishvili Tbilisi State University, 0186 Tbilisi, Georgia
[e] State Key Laboratory of Nuclear Physics and Technology, School of Physics, Peking University, Beijing 100871, China
[f] Yukawa Institute for Theoretical Physics, Kyoto University, Kyoto 606-8502, Japan

ARTICLE INFO

Article history:
Received 8 May 2020
Received in revised form 14 June 2020
Accepted 16 June 2020
Available online 22 June 2020
Editor: W. Haxton

ABSTRACT

The static quadrupole moments (SQMs) of nuclear chiral doublet bands are investigated for the first time taking the particle-hole configuration $\pi(1h_{11/2}) \otimes \nu(1h_{11/2})^{-1}$ with triaxial deformation parameters in the range $260° \leq \gamma \leq 270°$ as examples. The behavior of the SQM as a function of spin I is illustrated and analyzed. It is found that in the region of chiral vibrations the SQMs of doublet bands are strongly varying with I, whereas in the region of static chirality the SQMs of doublet bands are almost constant. Hence, the measurement of SQMs provides a new criterion for distinguishing the modes of nuclear chirality. Moreover, in the high-spin region the SQMs can be approximated by an analytic formula with a proportionality to $\cos\gamma$ for both doublet bands. This provides a way to extract experimentally the triaxial deformation parameter γ for chiral bands from the measured SQMs.

The phenomenon of nuclear chirality can appear in a fast rotating nucleus with a triaxially deformed core and high-j valence particles and holes [1]. In the body-fixed frame, the angular momenta of the valence particles and holes are aligned along the short and long axes of the triaxial core, respectively, while the angular momentum of the rotational core is aligned along the intermediate axis. Then, the left-handed and right-handed orientation of the three angular momenta are degenerate, and a spontaneous breaking of this chiral symmetry may happen. In the laboratory frame, due to the requirements of time-reversal invariance and quantum mechanical tunneling of the total angular momentum between the left-handed and right-handed configurations, the chiral symmetry is, however, restored. As a consequence, chiral doublet bands, i.e. pairs of nearly degenerate $\Delta I = 1$ bands with the same parity, are expected to be observable [1].

Up to now, more than 50 candidates for this phenomenon have been observed in the mass regions $A \approx 80$, 100, 130, and 190. For recent reviews on the subject, see Refs. [2–9] and the corresponding data tables in Ref. [10]. After the prediction [11] and confirmation [12] of multiple chiral doublet bands in a single nucleus, the investigation of chirality continues to be very interesting in nuclear structure physics.

Besides the energy spectra, the electromagnetic transition strengths are important observables for identifying nuclear chirality. Based on a model with the configuration $\pi(1h_{11/2}) \otimes \nu(1h_{11/2})^{-1}$ and a triaxial deformation parameter $\gamma = 30°$, the criteria for ideal nuclear chirality are according to Refs. [1,2,5,13–21] similar intra-band and inter-band reduced magnetic dipole ($M1$) and electric quadrupole ($E2$) transition strengths.

The search for additional observables that characterize nuclear chirality is still an interesting question. Very recently, the first measurement of the g-factor (gyromagnetic ratio) in a chiral band has been carried out for the bandhead of ^{128}Cs [22]. The g-factor can give important information on the relative orientation of the three angular momentum vectors of the particle, the hole, and the nuclear core. It can also be used to discern whether the three angular momentum vectors lie in a plane (planar configuration, known as chiral vibration) or whether they span the three-dimensional space (aplanar configuration, known as static chirality).

In this work the static (electric) quadrupole moments (SQMs) [also called spectroscopic quadrupole moments] of nuclear chiral doublet bands will be investigated for the first time. As will be seen from the following discussions, the SQM is related to the intrinsic deformation parameter (a static property) and the orientation of the total angular momentum (a dynamic property) of the nuclear system. The SQM provides some essential information about the charge distribution associated with the rotational mo-

* Corresponding author.
E-mail addresses: qbchen@pku.edu.cn (Q.B. Chen), nkaiser@ph.tum.de (N. Kaiser), meissner@hiskp.uni-bonn.de (U.-G. Meißner), mengj@pku.edu.cn (J. Meng).

https://doi.org/10.1016/j.physletb.2020.135568

tion, and it helps to discern whether the angular momenta have formed configurations related to chiral vibration or static chirality.

Our calculations are based on the particle rotor model (PRM), which has been widely used to describe chiral doublet bands and has achieved major successes in this respect [1,7,13,23–30]. It is a quantum mechanical model that combines the collective rotational motion and the intrinsic single-particle motions, describing the nuclear system in the laboratory frame. Its Hamiltonian is diagonalized in states with the total angular momentum as a good quantum number. The energy splitting and quantum mechanical tunneling probabilities between the doublet bands can be obtained directly from the diagonalization process. Actually, the basic input to the PRM can be obtained from covariant density functional theory (CDFT) [11,31], for practical applications, see Refs. [12,20,22,28,32–36]. Hence, the PRM can be used straightforwardly to investigate the SQMs of chiral doublet bands.

In the PRM the Hamiltonian for a system with one proton and one neutron coupled to a triaxial rigid (collective) rotor is composed as [1,7,13,23–30]

$$\hat{H}_{\rm PRM} = \hat{H}_{\rm coll} + \hat{H}_p + \hat{H}_n, \tag{1}$$

where $\hat{H}_{\rm coll}$ represents the Hamiltonian of the rigid rotor,

$$\hat{H}_{\rm coll} = \sum_{k=1}^{3} \frac{\hat{R}_k^2}{2\mathcal{J}_k} = \sum_{k=1}^{3} \frac{(\hat{I}_k - \hat{j}_{pk} - \hat{j}_{nk})^2}{2\mathcal{J}_k}, \tag{2}$$

with the index $k = 1, 2, 3$ referring to components along the three principal axes in the body-fixed frame. Here, $\hat{R}_k$ and $\hat{I}_k$ are the angular momentum operators of the collective rotor and the total nucleus, while $\hat{j}_{p(n)k}$ is the angular momentum operator of the valence proton (neutron). Moreover, the parameters $\mathcal{J}_k$ are the three principal moments of inertia.

The Hamiltonians $\hat{H}_p$ and $\hat{H}_n$ describe a single proton and neutron outside of the rotor. For a nucleon in a j-shell orbital, $\hat{H}_{p(n)}$ is given by

$$\hat{H}_{p(n)} = \pm\frac{C}{2}\Big\{\cos\gamma\Big[\hat{j}_3^2 - \frac{j(j+1)}{3}\Big] + \frac{\sin\gamma}{2\sqrt{3}}(\hat{j}_+^2 + \hat{j}_-^2)\Big\}, \tag{3}$$

where the sign $\pm$ refers to a particle or hole and γ is the triaxial deformation parameter. The coupling parameter C is proportional to the quadrupole deformation parameter β of the rotor.

The PRM Hamiltonian in Eq. (1) can be solved by diagonalization in the strong-coupling basis [37,38]

$$\begin{aligned}&|j_p\Omega_p j_n\Omega_n K, IM\rangle \\ &= \sqrt{\frac{1}{2}}\Big[|j_p\Omega_p\rangle|j_n\Omega_n\rangle|IMK\rangle \\ &\quad + (-1)^{I-j_p-j_n}|j_p-\Omega_p\rangle|j_n-\Omega_n\rangle|IM-K\rangle\Big],\end{aligned} \tag{4}$$

where I denotes the total angular momentum quantum number of the odd-odd nuclear system (rotor plus proton and neutron) and M (K) refers to the projection onto the z-axis (3-axis) in the laboratory (intrinsic) frame. Furthermore, $\Omega_{p(n)}$ is the quantum number for the 3-axis component of the valence nucleon angular momentum operator $\boldsymbol{j}_{p(n)}$ in the intrinsic frame, while the states $|IMK\rangle$ are represented in terms of three Euler angles $(\psi', \theta', \varphi')$ by the conventional Wigner-functions $\sqrt{\frac{2I+1}{8\pi^2}} D^I_{M,K}(\psi', \theta', \varphi')$. Under the requirement of the D_2 symmetry of a triaxial nucleus [37], K and Ω_p take the values: $K = -I, \ldots, I$ and $\Omega_p = -j_p, \ldots, j_p$. The quantum number Ω_n goes over the range $\Omega_n = -j_n, \ldots, j_n$ and it has to fulfill the condition that $K_R = K - \Omega_p - \Omega_n$ is a positive even integer.

The PRM eigenfunctions are expressed in the strong-coupling basis as

$$|IM\rangle = \sum_{K\Omega_p\Omega_n} f_{IK\Omega_p\Omega_n}|j_p\Omega_p j_n\Omega_n K, IM\rangle, \tag{5}$$

where the coefficients $f_{IK\Omega_p\Omega_n}$ are obtained by diagonalizing the Hamiltonian $\hat{H}_{\rm PRM}$. With the obtained wave functions the SQMs are calculated as [37,38]

$$Q(I) = \langle II|\hat{Q}_{20}|II\rangle, \tag{6}$$

where the quadrupole momentum operator in the laboratory frame $\hat{Q}_{20}$ is related to the intrinsic quadrupole moment $Q'_{2\nu}$ by

$$\hat{Q}_{20} = \sum_{\nu} D^2_{0,\nu} Q'_{2\nu}, \tag{7}$$

with $Q'_{20} = Q'_0\cos\gamma$, $Q'_{21} = Q'_{2-1} = 0$, $Q'_{22} = Q'_{2-2} = Q'_0\sin\gamma/\sqrt{2}$. Here, Q'_0 is an empirical quadrupole moment that is related to the axial deformation β by $Q'_0 = 3R_0^2 Z\beta/\sqrt{5\pi}$, where Z is the proton number and $R_0 = 1.2\,{\rm fm}\,A^{1/3}$. One can finally obtain the SQM for each band as

$$\begin{aligned}Q(I) = \langle II20|II\rangle &\sum_{\Omega_p\Omega_n}\sum_{KK'} f^*_{IK\Omega_p\Omega_n} f_{IK'\Omega_p\Omega_n} \\ &\times \sum_{\nu}\langle IK'2\nu|IK\rangle Q'_{2\nu}.\end{aligned} \tag{8}$$

The computation of the SQM is straightforward with the given PRM wave function. In the following, we give two alternative ways of calculating the SQM.

On the one hand, one consider the following relations between Wigner-functions $D^2_{0,\nu}$ in Eq. (7) and certain angular momentum operators when acting on the states $|II\rangle$ [39]

$$D^2_{0,0}|II\rangle = \frac{3\hat{I}_3^2 - I(I+1)}{(I+1)(2I+3)}|II\rangle, \tag{9}$$

$$D^2_{0,2}|II\rangle = \sqrt{\frac{3}{2}}\frac{\hat{I}_+^2}{(I+1)(2I+3)}|II\rangle, \tag{10}$$

$$D^2_{0,-2}|II\rangle = \sqrt{\frac{3}{2}}\frac{\hat{I}_-^2}{(I+1)(2I+3)}|II\rangle, \tag{11}$$

with the raising and lowering operators $\hat{I}_\pm = \hat{I}_1 \pm i\hat{I}_2$. Therefore, one gets a decomposition into two contributions

$$Q(I) = Q_0(I) + Q_2(I), \tag{12}$$

$$Q_0(I) = \frac{3\langle\hat{I}_3^2\rangle - I(I+1)}{(I+1)(2I+3)} Q'_0\cos\gamma, \tag{13}$$

$$Q_2(I) = \frac{\sqrt{3}(\langle\hat{I}_1^2\rangle - \langle\hat{I}_2^2\rangle)}{(I+1)(2I+3)} Q'_0\sin\gamma. \tag{14}$$

In the case of prolate deformation $\gamma = 0°$, and if the third component of the angular momentum $\langle\hat{I}_3\rangle = K$ is a good quantum number, the part $Q_2(I)$ vanishes and $Q(I)$ becomes

$$Q(I) = \frac{3K^2 - I(I+1)}{(I+1)(2I+3)} Q'_0. \tag{15}$$

This famous formula has already been given in textbooks (e.g., Refs. [37,38]). It is often used to extract the intrinsic quadrupole moment Q'_0 of an individual state from the measured $Q(I)$-values for an axially deformed nucleus.

On the other hand, if the z-axis in the laboratory frame is chosen along the angular momentum $\boldsymbol{I}$ (which is realized by $M = I$),

the Euler angles $(\psi', \theta', \varphi')$ and the tilted angles (θ, φ) are related in the following way

$$\theta = \theta', \quad \varphi = \pi - \varphi'. \tag{16}$$

Here, θ is the angle between the total spin $\boldsymbol{I}$ and the 3-axis, and the φ is the angle between the projection of total spin $\boldsymbol{I}$ onto the 1-2 plane and the 1-axis. With this connection one can express the quadrupole moment operator $\hat{Q}_{20}$ a function of θ and φ.

The Wigner-functions at $\psi' = 0$ have the form

$$D^2_{0,0}(0, \theta', \varphi') = \frac{1}{2}(3\cos^2\theta - 1), \tag{17}$$

$$D^2_{0,2}(0, \theta', \varphi') = \sqrt{\frac{3}{8}}\sin^2\theta e^{-2i\varphi}, \tag{18}$$

$$D^2_{0,-2}(0, \theta', \varphi') = \sqrt{\frac{3}{8}}\sin^2\theta e^{2i\varphi}, \tag{19}$$

and hence,

$$\hat{Q}_{20}(\theta, \varphi) = \frac{1}{2}(3\cos^2\theta - 1)Q'_0\cos\gamma + \frac{\sqrt{3}}{2}\sin^2\theta(\cos^2\varphi - \sin^2\varphi)Q'_0\sin\gamma. \tag{20}$$

Once the probability distribution of the orientation of the total angular momentum $\mathcal{P}(\theta, \varphi)$ (called azimuthal plot [40–42]) is known, the SQM can be calculated as a solid angle integral

$$Q(I) = \int_0^{\pi} \sin\theta d\theta \int_0^{2\pi} d\varphi\ \hat{Q}_{20}(\theta, \varphi)\mathcal{P}(\theta, \varphi). \tag{21}$$

Combining Eqs. (12) and (20), one can find interesting relationships between expectation values of the tilted angles (θ, φ) and the angular momentum components $\hat{I}_k$,

$$\langle\sin^2\theta\cos^2\varphi\rangle = \frac{\langle\hat{I}^2_1\rangle + (I+1)/2}{(I+1)(I+3/2)}, \tag{22}$$

$$\langle\sin^2\theta\sin^2\varphi\rangle = \frac{\langle\hat{I}^2_2\rangle + (I+1)/2}{(I+1)(I+3/2)}, \tag{23}$$

$$\langle\cos^2\theta\rangle = \frac{\langle\hat{I}^2_3\rangle + (I+1)/2}{(I+1)(I+3/2)}. \tag{24}$$

It follows immediately that

$$\langle\sin^2\theta\cos^2\varphi\rangle + \langle\sin^2\theta\sin^2\varphi\rangle + \langle\cos^2\theta\rangle = 1 \tag{25}$$

holds, consistent with the normalization of the PRM wave function. Especially, at $I = 0$ one has $\langle\hat{I}^2_k\rangle = 0$ and gets an isotropic angular distribution $\langle\sin^2\theta\cos^2\varphi\rangle = \langle\sin^2\theta\sin^2\varphi\rangle = \langle\cos^2\theta\rangle = 1/3$.

In the calculations of the chiral doublet bands for the configuration $\pi(1h_{11/2})^1 \otimes \nu(1h_{11/2})^{-1}$ the deformation parameter $\beta = 0.23$ is fixed and the chosen coupling coefficients are $C_p = 0.32$ MeV and $C_n = -0.32$ MeV, in accordance with standard values for the mass region $A \approx 130$. For the moments of inertia, the irrotational flow formula $\mathcal{J}_k = \mathcal{J}_0\sin^2(\gamma - 2k\pi/3)$ with $\mathcal{J}_0 = 30\ \hbar^2/\text{MeV}$ is used. In addition, the value $Q'_0 = 3.5\ e\text{b}$ is chosen for the empirical electric quadrupole moment.

The present studies focus on the following values of the triaxial deformation parameter: $\gamma = 270°$, $269°$, $267°$, $265°$, $263°$, and $260°$. With these specifications of γ, the 1-axis, 2-axis, and 3-axis are the short (s), long (l), and intermediate (m) axes of the triaxially deformed ellipsoid, respectively. Note that the moment of inertia $\mathcal{J}_m$ with respect to the m-axis is the largest for all selected γ-values. The moment of inertia $\mathcal{J}_s$ is equal to $\mathcal{J}_l$ at $\gamma = 270°$,

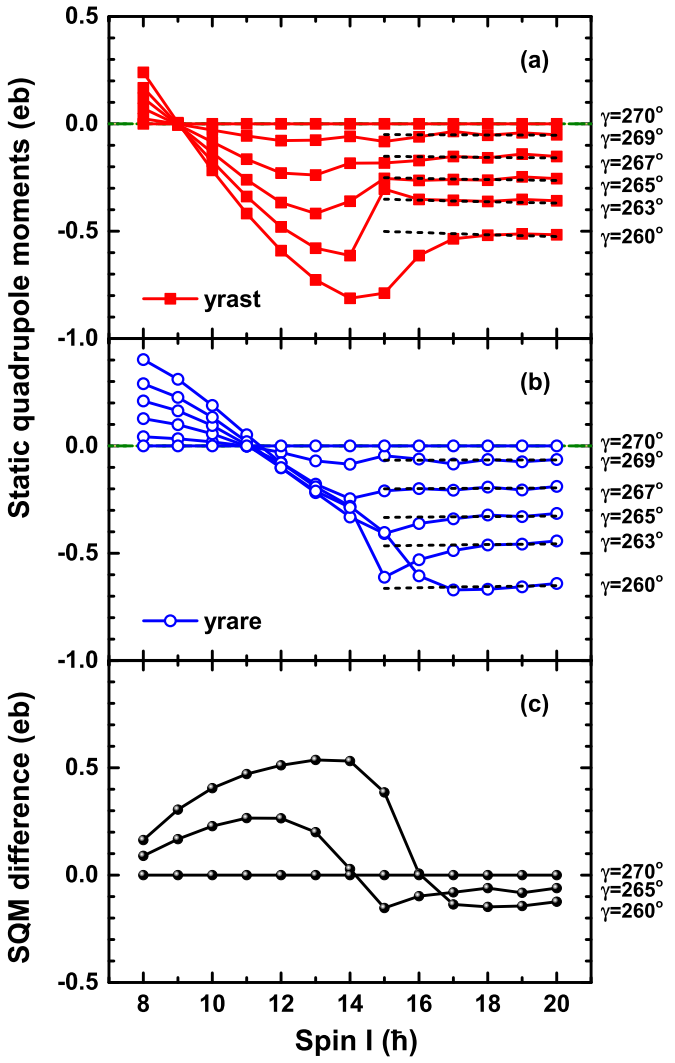

Fig. 1. Static quadrupole moments of yrast (a) and yrare (b) bands calculated in the PRM for the configuration $\pi(1h_{11/2})^1 \otimes \nu(1h_{11/2})^{-1}$ with $\gamma = 270°$, $269°$, $267°$, $265°$, $263°$, and $260°$. The lines for the yrast band are given by Eq. (26) and for the yrare band by Eq. (27). (c) The corresponding difference of static quadrupole moments between the yrare and yrast bands at $\gamma = 270°$, $265°$, $260°$.

while it is a bit larger than $\mathcal{J}_l$ for the other γ-values. Moreover, for the particle-hole configuration $\pi(1h_{11/2})^1 \otimes \nu(1h_{11/2})^{-1}$ with this range of γ, there occurs the so-called chiral geometry in a certain spin-region, according to the investigations presented in Refs. [1,17,27,29,41,43,44]. We refer to these papers for the corresponding results concerning energy spectra, electromagnetic transition probabilities, and the entire angular momentum geometry.

The corresponding SQMs of yrast and yrare bands as calculated in the PRM are shown in Fig. 1. Its contributions $Q_0(I)$ and $Q_2(I)$ as calculated by Eqs. (13) and (14) are shown in Fig. 2.

These two figures display the variation of the SQMs with the triaxial deformation parameter γ. At $\gamma = 270°$, the SQMs of the yrast and yrare bands are both zero over the entire spin region. The vanishing values of $Q_0(I)$ result from the fact that $Q_0(I)$ and $Q_2(I)$ are both zero. Note that $Q_0(I) = 0$ stems from the static property $\cos 270° = 0$, and $Q_2(I) = 0$ has a dynamical origin, namely $\langle\hat{I}^2_s\rangle = \langle\hat{I}^2_l\rangle$ as will be demonstrated in Fig. 3.

When γ deviates from $270°$, the values of $Q(I)$ do not vanish any longer. At several low-spins, the SQMs come out positive. With increasing spin, $Q(I)$ decreases first, then shows a rapid increase, and finally becomes almost constant. One can observe that

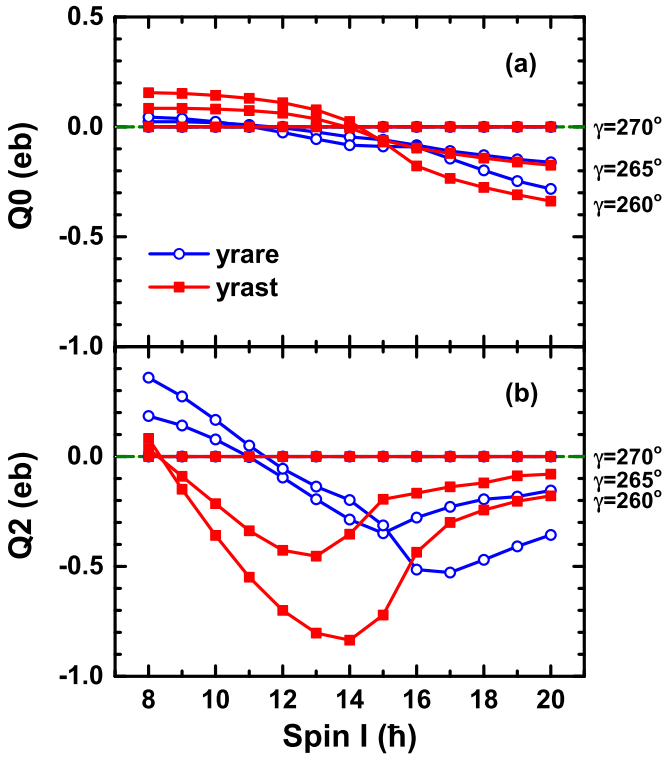

Fig. 2. Contributions to the static quadrupole moment $Q_0(I)$ (a) and $Q_2(I)$ (b) for doublet bands calculated in the PRM for the particle-hole configuration $\pi(1h_{11/2})^1 \otimes \nu(1h_{11/2})^{-1}$ with $\gamma = 270°$, 265°, and 260°.

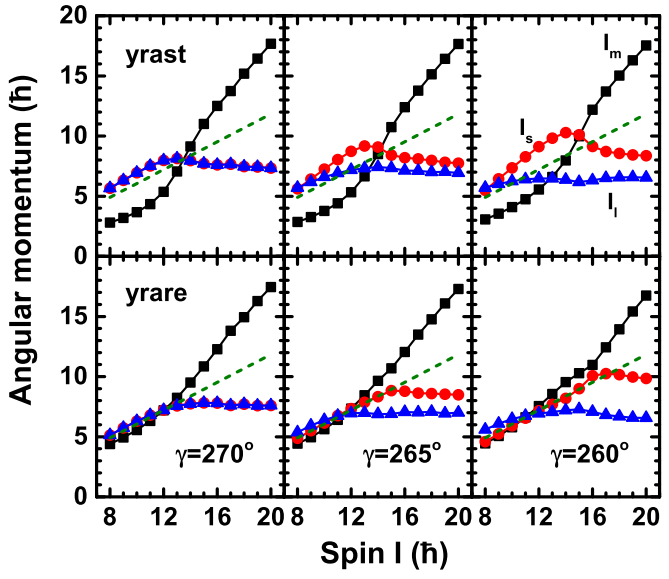

Fig. 3. Root mean-square values of the total angular momentum components along the short (s-, circles), long (l-, triangles), and intermediate (m-, squares) axes as functions of the spin I in the PRM for doublet bands at $\gamma = 270°$, 265°, and 260°. The dashed lines represent the average quantity $\sqrt{I(I+1)/3}$.

with decreasing deformation parameter γ, the static quadrupole moment $Q(I)$ decreases in the high-spin region.

An interesting finding about $Q(I)$ at high-spin I is that it can be well approximated by an analytic formula for both doublet bands. For the yrast band, the formula reads

$$Q(I) = \frac{3I^2 - I(I+1)}{(I+1)(2I+3)} Q_0' \cos\gamma, \tag{26}$$

while for the yrare band, it is

$$Q(I) = \frac{3(I+3/2)^2 - I(I+1)}{(I+1)(2I+3)} Q_0' \cos\gamma. \tag{27}$$

Using these relations, one can extract the triaxial deformation parameter (located in the range $240° \le \gamma \le 300°$) from the experimentally measured $Q(I)$-values as

$$\gamma = \arccos\left\{ \frac{Q(I)}{Q_0'} \frac{(I+1)(2I+3)}{3I^2 - I(I+1)} \right\} \tag{28}$$

for the yrast band, and

$$\gamma = \arccos\left\{ \frac{Q(I)}{Q_0'} \frac{(I+1)(2I+3)}{3(I+3/2)^2 - I(I+1)} \right\} \tag{29}$$

for the yrare band, assuming a common value of Q_0'.

Moreover, the above connections together with Eqs. (12)-(14) suggest that the three expectation values $\langle \hat{I}_k^2 \rangle$ of (squared) angular momentum components satisfy in the high-spin region the (approximate) relations,

$$\frac{\sqrt{3}(I^2 - \langle \hat{I}_m^2 \rangle)}{\langle \hat{I}_s^2 \rangle - \langle \hat{I}_l^2 \rangle} \approx \tan\gamma \tag{30}$$

for the yrast band, and

$$\frac{\sqrt{3}[(I+3/2)^2 - \langle \hat{I}_m^2 \rangle]}{\langle \hat{I}_s^2 \rangle - \langle \hat{I}_l^2 \rangle} \approx \tan\gamma \tag{31}$$

for the yrare band.

In order to understand better the behavior of the $Q(I)$-values in Fig. 1, we have also shown the individual contributions $Q_0(I)$ and $Q_2(I)$ at $\gamma = 270°$, 265°, and 260°. One can see that generally $Q_0(I)$ is much smaller than $Q_2(I)$, due to the suppression by the factor $\cos\gamma$ (a static property). Hence, the behavior of $Q(I)$ as a function of spin I is mainly determined by $Q_2(I)$. In particular, this explains the decreasing trend visible in the low-spin region.

In order to present more details, we show in Fig. 3 the root mean-square values of the total angular momentum components along the s-axis, l-axis, and m-axis ($I_s = \langle \hat{I}_s^2 \rangle^{1/2}$, $I_l = \langle \hat{I}_l^2 \rangle^{1/2}$, and $I_m = \langle \hat{I}_m^2 \rangle^{1/2}$) as functions of the spin I for the doublet bands at $\gamma = 270°$, 265°, and 260°. The corresponding orientation components, defined as the expectation values $\langle \sin^2\theta \cos^2\varphi \rangle$, $\langle \sin^2\theta \sin^2\varphi \rangle$, and $\langle \cos^2\theta \rangle$ according to Eqs. (22)-(24) are displayed in Fig. 4. The dashed lines at height $\sqrt{I(I+1)/3}$ and 1/3 refer to completely isotropic distributions.

Obviously, the equalities $I_s = I_l$ and $\langle \sin^2\theta \cos^2\varphi \rangle = \langle \sin^2\theta \sin^2\varphi \rangle$ hold at $\gamma = 270°$. This is a consequence of the symmetric configuration of the proton-particle (mainly aligning along the s-axis) and the neutron-hole (mainly aligning along the l-axis) as well as the equivalence of the moments of inertia with respect to the s-axis and l-axis. As mentioned above, this coincidence causes $Q_2(I) = 0$ at $\gamma = 270°$.

When γ deviates from 270°, I_s is no longer equal to I_l. For the yrast band, I_s is in general larger than I_l since $\mathcal{J}_s > \mathcal{J}_l$. Consequently, $Q_2(I)$ of the yrast band becomes negative, noting that $\sin\gamma$ is negative. For the yrare band, I_s is smaller than I_l in the region $I \le 12\hbar$. Correspondingly, the contribution $Q_2(I)$ as well as the total $Q(I)$ are positive as shown in Figs. 2 and 1. At $I \ge 13\hbar$, one has $I_s > I_l$, similar to the situation in the yrast band. These features generate the (chiral) picture of a left-handed and a right-handed configuration in the body-fixed frame in the spin region $15 \le I \le 18\hbar$.

The component I_m increases with spin. For the yrast band, in the region with $I \le 14\hbar$ and $I_m < \sqrt{I(I+1)/3}$, corresponding to

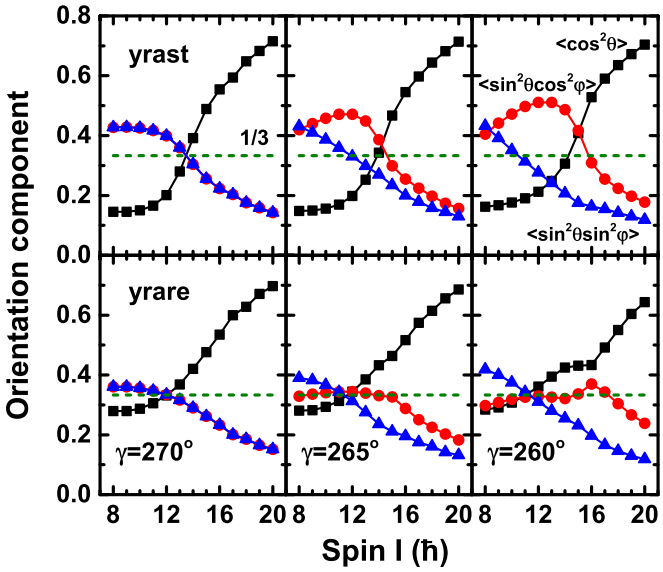

Fig. 4. Expectation values of $\langle \sin^2\theta \cos^2\varphi \rangle$, $\langle \sin^2\theta \sin^2\varphi \rangle$, and $\langle \cos^2\theta \rangle$ derived from Eqs. (22)-(24) for the doublet bands at $\gamma = 270°$, 265°, and 260°. The dashed line represents the isotropic average value 1/3.

$\langle \cos^2\theta \rangle < 1/3$, the total angular momentum is located close to the *sl*-plane. This gives positive $Q_0(I)$-values as shown in Fig. 2 (noting that $\cos\gamma$ is negative). In this region, I_m is smaller than I_s and I_l. This is due to the fact that the collective rotor motion has just started at the bandhead of the doublet bands. The component I_m is larger in the yrare band than in the yrast band, which can be attributed to the oscillations of the total angular momentum between the left-handed and the right-handed configuration (about the *sl*-plane). This phenomenon is known as the chiral vibration. Accordingly, the contribution $Q_0(I)$ of the static quadrupole moment is smaller in the yrare band than in the yrast band, as shown in Fig. 2. In the spin region $15 \leq I \leq 18\hbar$, the component I_m and $\langle \cos^2\theta \rangle$ behave similarly in both doublet bands, which corresponds to the phenomenon of static chirality. Consequently, the static quadrupole moments $Q(I)$ in both doublet bands are close to each other in this spin region.

In Fig. 1, we show furthermore the difference of SQMs between the yrare and yrast bands at deformation parameters $\gamma = 270°$, 265°, and 260°. According to the above analysis, when γ deviates from 270°, the differences of the SQMs between the doublet bands can be interpreted as the chiral vibration, and the similar SQMs are attributed to the static chirality. Therefore, a measurement of static quadrupole moments can provide a new criterion for nuclear chirality.

In summary, the SQMs of chiral doublet bands have been investigated for the first time taking the particle-hole configuration $\pi(1h_{11/2}) \otimes \nu(1h_{11/2})^{-1}$ with triaxial deformation parameters in the range $260° \leq \gamma \leq 270°$ as examples. The behavior of the SQMs as a function of spin I is illustrated by analyzing the components of the total angular momentum. Pronounced differences of the SQMs between the doublet bands are attributed to the chiral vibration, whereas their similarity signifies the static chirality. This provides a new criterion to distinguish the modes of nuclear chirality. Moreover, it is found that in the high-spin region the SQMs can be approximated by an analytic formula with a proportionality to $\cos\gamma$ for both doublet bands. It provides a way to extract experimentally the triaxial deformation parameter γ of chiral bands from the measured SQMs. In view of this connection, experimental measurements of SQMs for the chiral doublet bands are strongly suggested.

Declaration of competing interest

The authors declare that they have no known competing financial interests or personal relationships that could have appeared to influence the work reported in this paper.

Acknowledgements

One of the authors (Q.B.C.) thanks S. Frauendorf and I. Hamamoto for helpful discussions. This work has been supported in parts by Deutsche Forschungsgemeinschaft (DFG) and National Natural Science Foundation of China (NSFC) through funds provided by the Sino-German CRC 110 "Symmetries and the Emergence of Structure in QCD" (DFG Grant No. TRR110 and NSFC Grant No. 11621131001), the National Key R&D Program of China (Contract No. 2017YFE0116700 and No. 2018YFA0404400), the NSFC under Grant No. 11935003, and the State Key Laboratory of Nuclear Physics and Technology of Peking University (Grant No. NPT2020ZZ01). The work of U.-G.M. was also supported by the Chinese Academy of Sciences (CAS) through a President's International Fellowship Initiative (PIFI) (Grant No. 2018DM0034) and by the VolkswagenStiftung (Grant No. 93562).

References

[1] S. Frauendorf, J. Meng, Nucl. Phys. A 617 (1997) 131.
[2] J. Meng, S.Q. Zhang, J. Phys. G, Nucl. Part. Phys. 37 (2010) 064025.
[3] J. Meng, Q.B. Chen, S.Q. Zhang, Int. J. Mod. Phys. E 23 (2014) 1430016.
[4] R.A. Bark, E.O. Lieder, R.M. Lieder, E.A. Lawrie, J.J. Lawrie, S.P. Bvumbi, N.Y. Kheswa, S.S. Ntshangase, T.E. Madiba, P.L. Masiteng, et al., Int. J. Mod. Phys. E 23 (2014) 1461001.
[5] J. Meng, P.W. Zhao, Phys. Scr. 91 (2016) 053008.
[6] A.A. Raduta, Prog. Part. Nucl. Phys. 90 (2016) 241.
[7] K. Starosta, T. Koike, Phys. Scr. 92 (2017) 093002.
[8] S. Frauendorf, Phys. Scr. 93 (2018) 043003.
[9] Q.B. Chen, J. Meng, Nucl. Phys. News 30 (2020) 11.
[10] B.W. Xiong, Y.Y. Wang, At. Data Nucl. Data Tables 125 (2019) 193.
[11] J. Meng, J. Peng, S.Q. Zhang, S.-G. Zhou, Phys. Rev. C 73 (2006) 037303.
[12] A.D. Ayangeakaa, U. Garg, M.D. Anthony, S. Frauendorf, J.T. Matta, B.K. Nayak, D. Patel, Q.B. Chen, S.Q. Zhang, P.W. Zhao, et al., Phys. Rev. Lett. 110 (2013) 172504.
[13] T. Koike, K. Starosta, I. Hamamoto, Phys. Rev. Lett. 93 (2004) 172502.
[14] E. Grodner, J. Srebrny, A.A. Pasternak, I. Zalewska, T. Morek, C. Droste, J. Mierzejewski, M. Kowalczyk, J. Kownacki, M. Kisielinski, et al., Phys. Rev. Lett. 97 (2006) 172501.
[15] D. Tonev, G. de Angelis, P. Petkov, A. Dewald, S. Brant, S. Frauendorf, D.L. Balabanski, P. Pejovic, D. Bazzacco, P. Bednarczyk, et al., Phys. Rev. Lett. 96 (2006) 052501.
[16] S. Mukhopadhyay, D. Almehed, U. Garg, S. Frauendorf, T. Li, P.V.M. Rao, X. Wang, S.S. Ghugre, M.P. Carpenter, S. Gros, et al., Phys. Rev. Lett. 99 (2007) 172501.
[17] B. Qi, S.Q. Zhang, S.Y. Wang, J.M. Yao, J. Meng, Phys. Rev. C 79 (2009) 041302(R).
[18] E. Grodner, I. Sankowska, T. Morek, S.G. Rohozinski, C. Droste, J. Srebrny, A.A. Pasternak, M. Kisielinski, M. Kowalczyk, J. Kownacki, et al., Phys. Lett. B 703 (2011) 46.
[19] D. Tonev, M.S. Yavahchova, N. Goutev, G. de Angelis, P. Petkov, R.K. Bhowmik, R.P. Singh, S. Muralithar, N. Madhavan, R. Kumar, et al., Phys. Rev. Lett. 112 (2014) 052501.
[20] E.O. Lieder, R.M. Lieder, R.A. Bark, Q.B. Chen, S.Q. Zhang, J. Meng, E.A. Lawrie, J.J. Lawrie, S.P. Bvumbi, N.Y. Kheswa, et al., Phys. Rev. Lett. 112 (2014) 202502.
[21] N. Rather, P. Datta, S. Chattopadhyay, S. Rajbanshi, A. Goswami, G.H. Bhat, J.A. Sheikh, S. Roy, R. Palit, S. Pal, et al., Phys. Rev. Lett. 112 (2014) 202503.
[22] E. Grodner, J. Srebrny, C. Droste, L. Próchniak, S.G. Rohoziński, M. Kowalczyk, M. Ionescu-Bujor, C.A. Ur, K. Starosta, T. Ahn, et al., Phys. Rev. Lett. 120 (2018) 022502.
[23] J. Peng, J. Meng, S.Q. Zhang, Phys. Rev. C 68 (2003) 044324.
[24] S.Q. Zhang, B. Qi, S.Y. Wang, J. Meng, Phys. Rev. C 75 (2007) 044307.
[25] B. Qi, S.Q. Zhang, J. Meng, S.Y. Wang, S. Frauendorf, Phys. Lett. B 675 (2009) 175.
[26] E.A. Lawrie, O. Shirinda, Phys. Lett. B 689 (2010) 66.
[27] Q.B. Chen, K. Starosta, T. Koike, Phys. Rev. C 97 (2018) 041303(R).
[28] Q.B. Chen, B.F. Lv, C.M. Petrache, J. Meng, Phys. Lett. B 782 (2018) 744.
[29] Q.B. Chen, N. Kaiser, U.-G. Meißner, J. Meng, Phys. Rev. C 99 (2019) 064326.
[30] Y.Y. Wang, S.Q. Zhang, P.W. Zhao, J. Meng, Phys. Lett. B 792 (2019) 454.
[31] J. Meng (Ed.), Relativistic Density Functional for Nuclear Structure, International Review of Nuclear Physics, vol. 10, World Scientific, Singapore, 2016.

[32] I. Kuti, Q.B. Chen, J. Timár, D. Sohler, S.Q. Zhang, Z.H. Zhang, P.W. Zhao, J. Meng, K. Starosta, T. Koike, et al., Phys. Rev. Lett. 113 (2014) 032501.
[33] C. Liu, S.Y. Wang, R.A. Bark, S.Q. Zhang, J. Meng, B. Qi, P. Jones, S.M. Wyngaardt, J. Zhao, C. Xu, et al., Phys. Rev. Lett. 116 (2016) 112501.
[34] C.M. Petrache, Q.B. Chen, S. Guo, A.D. Ayangeakaa, U. Garg, J.T. Matta, B.K. Nayak, D. Patel, J. Meng, M.P. Carpenter, et al., Phys. Rev. C 94 (2016) 064309.
[35] J. Peng, Q.B. Chen, Phys. Lett. B 793 (2019) 303.
[36] B.F. Lv, C.M. Petrache, Q.B. Chen, J. Meng, A. Astier, E. Dupont, P. Greenlees, H. Badran, T. Calverley, D.M. Cox, et al., Phys. Rev. C 100 (2019) 024314.
[37] A. Bohr, B.R. Mottelson, Nuclear Structure, vol. II, Benjamin, New York, 1975.
[38] P. Ring, P. Schuck, The Nuclear Many Body Problem, Springer Verlag, Berlin, 1980.
[39] E.R. Marshalek, Nucl. Phys. A 275 (1977) 416.
[40] F.Q. Chen, Q.B. Chen, Y.A. Luo, J. Meng, S.Q. Zhang, Phys. Rev. C 96 (2017) 051303(R).
[41] Q.B. Chen, J. Meng, Phys. Rev. C 98 (2018) 031303(R).
[42] E. Streck, Q.B. Chen, N. Kaiser, U.-G. Meißner, Phys. Rev. C 98 (2018) 044314.
[43] Q.B. Chen, J.M. Yao, S.Q. Zhang, B. Qi, Phys. Rev. C 82 (2010) 067302.
[44] H. Zhang, Q.B. Chen, Chin. Phys. C 40 (2016) 024101.